J Physiol 591.17 (2013) pp 4287–4299

The Journal of Physiology

Cardiac calcium signalling pathologies associated with defective calmodulin regulation of type 2 ryanodine receptor

Juan José Arnáiz-Cot[1], Brooke James Damon[1,2], Xiao-Hua Zhang[1], Lars Cleemann[1], Naohiro Yamaguchi[1,2], Gerhard Meissner[3] and Martin Morad[1,2]

[1]*Cardiac Signaling Center, University of South Carolina, Medical University of South Carolina and Clemson University, Charleston, SC 29425, USA*
[2]*Department of Regenerative Medicine and Cell Biology, Medical University of South Carolina, Charleston, SC 29425, USA*
[3]*Department of Biochemistry and Biophysics, School of Medicine, University of North Carolina, Chapel Hill, NC 27599-7260, USA*

Abstract Cardiac ryanodine receptor (RyR2) is a homotetramer of 560 kDa polypeptides regulated by calmodulin (CaM), which decreases its open probability at diastolic and systolic Ca^{2+} concentrations. Point mutations in the CaM-binding domain of RyR2 (W3587A/L3591D/F3603A, $RyR2^{ADA}$) in mice result in severe cardiac hypertrophy, poor left ventricle contraction and death by postnatal day 16, suggesting that CaM inhibition of RyR2 is required for normal cardiac function. Here, we report on Ca^{2+} signalling properties of enzymatically isolated, Fluo-4 dialysed whole cell clamped cardiac myocytes from 10–15-day-old wild-type (WT) and homozygous $Ryr2^{ADA/ADA}$ mice. Spontaneously occurring Ca^{2+} spark frequency, measured at −80 mV, was 14-fold lower in mutant compared to WT myocytes. I_{Ca}, though significantly smaller in mutant myocytes, triggered Ca^{2+} transients that were of comparable size to those of WT myocytes, but with slower activation and decay kinetics. Caffeine-triggered Ca^{2+} transients were about three times larger in mutant myocytes, generating three- to four-fold bigger Na^{+}-Ca^{2+} exchanger NCX currents (I_{NCX}). Mutant myocytes often exhibited Ca^{2+} transients of variable size and duration that were accompanied by similarly alternating and slowly activating I_{NCX}. The data suggest that $RyR2^{ADA}$ mutation produces significant reduction in I_{Ca} density and I_{Ca}-triggered Ca^{2+} release gain, longer but infrequently occurring Ca^{2+} sparks, larger sarcoplasmic reticulum Ca^{2+} loads, and spontaneous Ca^{2+} releases accompanied by activation of large and potentially arrhythmogenic inward I_{NCX}.

(Received 29 March 2013; accepted after revision 5 July 2013; first published online 8 July 2013)
Corresponding author M. Morad: Cardiac Signaling Center, 173 Ashley Ave, Bioengineering Building, Room 306, Charleston, SC 29403, USA. Email: moradm@musc.edu

Abbreviations CaM, calmodulin; CaMKII, CaM-dependent protein kinase II; CICR, I_{Ca}-triggered Ca^{2+} release; I_{Ca}, Ca^{2+} current; I_{NCX}, current generated by the Na^{+}-Ca^{2+} exchanger; NCX, Na^{+}-Ca^{2+} exchanger; PKA, protein kinase A; RyR2, type 2 ryanodine receptor; SR, sarcoplasmic reticulum.

Introduction

Excitation–contraction coupling in cardiac muscle is initiated by activation of voltage-gated Ca^{2+} channel and influx of Ca^{2+} that in turn triggers Ca^{2+} release from the ryanodine receptors (RyR2) of the sarcoplasmic reticulum (SR). The regulation of Ca^{2+} release from RyR2 is mediated not only by influx of Ca^{2+}, but also by the host of regulatory proteins bound to cytoplasmic domains of RyR2s that include calmodulin (CaM), protein kinase A (PKA), FK506-binding protein (FKBP12.6), CaM-dependent protein kinase (CaMKII), protein phosphatases (calcineurin), and junctional and luminal SR proteins junctin, triadin and calsequestrin (Franzini-Armstrong & Protasi, 1997; Lanner *et al.* 2010). CaM is a small cytoplasmic Ca^{2+} binding protein, which regulates the RyR2s either by its direct binding to RyR2 or indirectly by regulating other proteins, CaMKII and CaM-stimulated protein phosphatase (calcineurin) (Balshaw *et al.* 2002; Saimi & Kung, 2002; Maier & Bers, 2007). In addition, RyR2 seems also to be regulated by cytosolic Ca^{2+}, Mg^{2+} and ATP (Meissner, 1994; Fill & Copello, 2002). The regulation of Ca^{2+} signalling by CaM

J. J. Arnáiz-Cot and B. J. Damon equally contributed to the experimental work

DOI: 10.1113/jphysiol.2013.256123

becomes somewhat more intricate as CaM also regulates two other proteins of the Ca^{2+} release and uptake pathway, namely the voltage-activated Ca^{2+} channel (Ca_v 1.2) of the surface membrane (Anderson *et al.* 1994; Tang *et al.* 2002), and Ca^{2+}-ATPase (SERCA2a) of the SR (Simmerman & Jones, 1998).

It has been already reported that CaM decreases the open probability of RyR2 and that deletion of amino acid residues 3583–3603 of RyR2 eliminates CaM binding and its regulation (Yamaguchi *et al.* 2003). To explore the role of CaM regulation of RyR2 *in vivo*, a mouse model was generated that expressed RyR2s with three amino acid replacements (RyR2-W3587A/L3591D/F3603A, $RyR2^{ADA}$) that impaired CaM regulation *in vivo* (Yamaguchi *et al.* 2007). The homozygous expression of $RyR2^{ADA}$ in mice resulted in larger hearts, severe cardiac hypertrophy, impaired left ventricle contraction and significant bradycardia (461 ± 19 *vs.* 598 ± 21 beats per minute), leading to death by postnatal day 16 (Yamaguchi *et al.* 2007). Cardiac hypertrophy and impaired left ventricle contraction were prominent in $Ryr2^{ADA/ADA}$ mice at postnatal day 1, and gene remodelling associated with cardiac hypertrophy was observed at embryonic day 16.5. The results suggest a significant role for CaM regulation of RyR2 in early development of the heart (Yamaguchi *et al.* 2007, 2011). In single channel recordings of RyR2, at high Ca^{2+} concentrations, exogenous application of CaM (1 μM) to the *cis* side of the bilayers, while reducing RyR2 open probability of wild-type (WT) had little or no effect on the mutant RyR2 (Yamaguchi *et al.* 2007).

In this study, the locus and extent of Ca^{2+} signalling defect affected by this mutation were explored in voltage-clamped myocytes to determine whether impaired Ca^{2+} signalling was responsible for cardiac failure and early death of the homozygous mice.

Methods

Mice

$RyR2^{ADA}$ mice were generated and established as described previously (Yamaguchi *et al.* 2007). Heterozygous mice ($Ryr2^{+/ADA}$) were at least 10 times backcrossed to 129/svev genetic background and were used for breeding to obtain WT and homozygous ($Ryr2^{ADA/ADA}$) mice. As homozygous mice die within 2–3 weeks, we used 10–15-day-old mice in the present study. All protocols were approved by Medical University of South Carolina Institutional Animal Care and Use Committees.

Cell isolation procedure

Single cardiomyocytes were prepared by enzymatic dissociation using modification of previously published methods (Mitra & Morad, 1985). Mice were injected with heparin (500 IU, I.P.) and anaesthetized with isoflurane. After sedation, the heart was excised and placed in a dish filled with 2 mM Ca^{2+} Tyrode's solution at ambient temperature containing (in mM): 10 Hepes, 0.33 Na_2HPO_4, 110 NaCl, 1 $MgCl_2$, 30 taurine, 15.4 L-glutamic acid and 10 glucose. Hearts were cannulated above the aortic valve and infused with Tyrode's solution with 2 mM Ca^{2+} for 1 min (3 ml min^{-1}) to clean blood from the tissue and then transferred to a Langendorf flow system. Hearts were perfused on the Langendorf apparatus for 6 min with Ca^{2+}-free Tyrode (37°C, pH 7.4, at 2 ml min^{-1} for controls, 3 ml min^{-1} for $Ryr2^{ADA/ADA}$ mice) containing 10 μM Blebbistatin. Subsequently, hearts were digested by perfusing collagense II (657 U ml^{-1}, Worthington, Lakewood, NJ, USA, lot 49H11299) and 2.5% trypsin (0.3 mg ml^{-1}) enzymes dissolved in Tyrode's solution (containing 12.5 μM $CaCl_2$ and 10 μM Blebbistatin) for 7–10 min until the tissue became soft to the touch or a sudden increase in flow rate occurred indicating effective tissue digestion. To halt enzymatic digestion, hearts were then perfused for 5 min with Ca^{2+}-free Tyrode's solution containing 10% foetal bovine serum and 10 μM Blebbistatin. Once enzymes were effectively washed from the tissue, the ventricles were cut into large pieces and placed in a 15 ml conical tube containing 2.5 ml of same solution and placed in a 37°C water bath. To avoid Ca^{2+} overload, Ca^{2+} was slowly reintroduced to the cells in a step-wise fashion. Every 4 min, the contents of the tube was gently mixed by inversion and $CaCl_2$ was added to the cells to increase the concentration from 12.5 μM to 62 μM, 112 μM, 212 μM, 500 μM and finally 1 mM. At this point, cells were allowed to settle by gravity for 10 min in the bath and then the pellet was re-suspended in 10 ml Tyrode with 1 mM Ca^{2+} and filtered to obtain single cells with a 70 μm filter (BD Biosciences, San Jose, CA, USA, Ref 354232). The filtered single cells were then plated on laminin-coated (10 μg ml^{-1}) glass coverslips and were allowed to recover and adhere fully for at least 2 h before their use in electrophysiological and imaging experiments.

Whole cell recordings of membrane currents

Membrane currents were measured in the whole cell configuration of the patch clamp technique (Hamill *et al.* 1981) using a DAGAN 8900 amplifier (Dagan Corp., Minneapolis, MN, USA) and data were acquired through the Digidata 1320A digitizer board (Axon Instruments, Foster City, CA, USA) with a sampling frequency of 10 kHz. The measured series resistance was approximately three times the pipette resistance and was electronically compensated through the amplifier. Patch electrodes were fabricated from borosilicate capillary glass with filament (1B150F-4; World Precision Instruments, Sarasota, FL, USA) and pulled using a Brown Flaming type pipette

puller (model P-87; Sutter Company, Novato, CA, USA) to a tip resistance of 3–7 MΩ when filled with a Cs^+-based internal solution. This solution contained (in mM): 127 CsCl, 5 tetraethylammonium chloride, 5 NaCl, 10 Hepes, 5 MgATP, 5 glucose with different additions of Ca^{2+} and Ca^{2+} probes suitable for whole cell Ca^{2+} measurements or confocal Ca^{2+} imaging. pH was titrated to 7.2 with CsOH. The standard external solution was composed of (in mM): 137 NaCl, 5.4 KCl, 1 $MgCl_2$, 10 Hepes, 2 $CaCl_2$, 2 glucose and titrated to pH 7.4 with NaOH. Ag-Cl ground and inner pipette electrodes were used and seal resistance before patch rupture ranged from 2 to 10 GΩ. A multibarrelled perfusion system (Cleemann & Morad, 1991) was used for application of K^+-free external solutions during recording of membrane currents and for rapid (∼50 ms) application of caffeine (10 mM). The generation of voltage clamp protocols and data acquisition was controlled by pCLAMP software (version 10.2; Axon Instruments, Inc.). Three clamp pulse protocols were used: (1) holding the membrane potential at −80 mV while caffeine-induced Ca^{2+} transients and the associated membrane current (I_{NCX}) were measured; (2) pulse protocols of various magnitudes and durations were applied from holding potentials of −80 or −60 mV to activate Ca^{2+} currents (I_{Ca}); and (3) Ca^{2+} sparks or spontaneous Ca^{2+} waves were monitored at rapid imaging frame rates at holding potentials of −80 mV. The pCLAMP software provided automated measurements of membrane capacitance using 10 mV test pulses from a holding potential of −60 mV. The accurate detection of I_{NCX} was facilitated by choosing cells with little or no leak currents and by suppression of K^+ currents by the use of a K^+-free external solution and a Cs^+-based internal solution with added tetraethylammonium. Furthermore, the leak currents were not digitally subtracted by the P/N method to avoid suppression of maintained components of I_{NCX}. All the experiments were performed at room temperature (∼25°C).

Global intracellular Ca^{2+} measurements

Intracellular Ca^{2+} activity was measured according to previous methods (Cleemann & Morad, 1991) using a dialysing pipette solution with addition of 0.5 mM $CaCl_2$ and 0.5 mM of the fluorescent Ca^{2+}-indicator dye K_5Fura-2. Briefly, ultraviolet light originated from a 100 W mercury arc lamp, was split into two beams by a mirror vibrating at 1200 Hz for high time resolution and alternately passed through excitation filters above and below the isosbestic point (380/14 and 340/20 nm) before they were recombined to allow ratiometric detection of Ca^{2+}. The parameter, F, plotted in these experiments (Figs 3–6 and 8) is the ratio of two signals obtained with excitation at wavelengths where Ca^{2+} respectively increases and decreases the intensity of fluorescent light. To enhance sensitivity, background fluorescence from the pipette solution was eliminated by removing the patch pipette from the field of view of the detector with an adjustable iris.

Two-dimensional confocal imaging

The time course of local Ca^{2+} signals was measured in voltage-clamped cardiomyocytes with Fluo-4 using a Noran Odyssey XL rapid two-dimensional laser scanning confocal microscopy system (Noran Instruments, Madison, WI, USA) attached to a Zeiss Axiovert TV135 inverted microscope fitted with an ×63 water-immersion objective lens. In these experiments, the dialysing solutions contained additions of either: (1) 1 mM EGTA, 1 mM K_5Fluo-4 and 0.6 mM $CaCl_2$, or (2) 0.5 mM K_5Fluo-4 and 0.2 mM $CaCl_2$. The excitation wavelength of the argon ion laser was set to 488 nm, and fluorescence emission was measured at wavelengths > 515 nm. Cells were imaged confocally at 30–120–240 frames s^{-1} depending on the experimental requirement. To reduce photobleaching, the laser beam used for excitation of Fluo-4 was electronically shuttered and triggered to open on command by the pClamp program only during acquisition of data. The average resting fluorescence intensity (F_0) was calculated from several frames measured immediately before voltage clamp depolarization or drug application or from selected frames without indication of spontaneous Ca^{2+} signals in the form of sparks or waves. Images were filtered by 2 pixel × 2 pixel averaging. The amplitudes of the Ca^{2+}-dependent cellular fluorescence signals were quantified as $\Delta F/F_0$, where ΔF is the change in fluorescence. This type of normalization could be applied both to the integrated signals from the entire cell (Fig. 2AC) and to the generation of ratiometric images where both F_0 and ΔF were measured locally (Figs 2*B* and *D* and 7*A* and *C*).

Membrane structures were measured in live cells with the Noran Odyssey XL confocal microscope using the lipophilic potentiometric dye di-2 ANEPEQ (Fig. 1*C*, bottom). For immunolabelling of proteins, the isolated mouse cardiomyocytes were fixed with 100% methanol for 10 min at 4°C and were blocked with 1% bovine serum albumin and 0.1% Triton-X100 in phosphate-buffered saline for 1 h at room temperature. Primary and secondary antibodies for immunostaining were C3–33 monoclonal antibody (Thermo, Waltham, MA, USA) and fluorescein isothiocyanate-conjugated antimouse IgG antibody (for RyR2) and π antibody and Texas red conjugated antirabbit IgG antibody (for NCX). The secondary fluorescent antibodies were from Jackson ImmunoResearch (West Grove, PA, USA) and were imaged on a Leica SP5 confocal microscope.

Chemicals

Mg-ATP and caffeine were from Sigma (St. Louis, MO, USA), and Fura-2 pentapotassium salt from Molecular Probes (Eugene, OR, USA).

Data analysis and statistics

Analysis of ion current amplitude was made with the CLAMPFIT module of pClamp 10.2 software. Data are reported as means ± S.E. Comparisons were done using Student's unpaired *t* test with *P* values indicated in the figures.

Results

Mutation of type 2 ryanodine receptor at the calmodulin-binding site

It has been already reported that homozygote mice carrying $RyR2^{ADA}$ mutation that causes reduced CaM binding to RyR2s, develop significant cardiac hypertrophy at postnatal day 1 compared to WT mice, and die within 2–3 weeks of birth (Yamaguchi *et al.* 2007, 2011). Functional evidence for ineffective CaM binding is based on findings that 1 μM CaM failed to decrease the mean open probability of $RyR2^{ADA}$, when added to *cis* (cytoplasmic) side of the bilayers containing the channel, as it did when WT RyR2 was incorporated in to the bilayers. Kinetic analysis revealed no significant differences between CaM-depleted WT and mutant channels in the number of channel events and mean open or closed times (Yamaguchi *et al.* 2007). Figure 1*A* shows a schematic representation of CaM-binding domain of RyR2 vis-à-vis some of the other well known regulatory phosphorylation and Ca^{2+} binding sites of this protein. Figure 1*B* compares representative images of two hearts obtained from WT and mutant mice at 11 days of life confirming massive cardiac hypertrophy (Yamaguchi *et al.* 2007). Figure 1*C* compares immunofluorescent distribution of RyR2, and NCX proteins, as well as membrane staining with a voltage-sensitive dye of three pairs of ventricular myocytes from WT and mutant mice. While the membrane staining (Mem) shows both the surface membrane and the sarcomeric pattern of its t-tubular invaginations, it is noticeable that NCX staining is most prominent in the former and RyR2-staining confined to the latter. Deformation of t-tubules is apparent in hypertrophied myocytes from mutant mice (arrows), especially when using the voltage-sensitive fluorescent dye. There was also considerable non-uniformity in the extent of cellular hypertrophy between myocytes. Compare for instance, NCX immunostained myocyte pairs with RyR2-stained pairs.

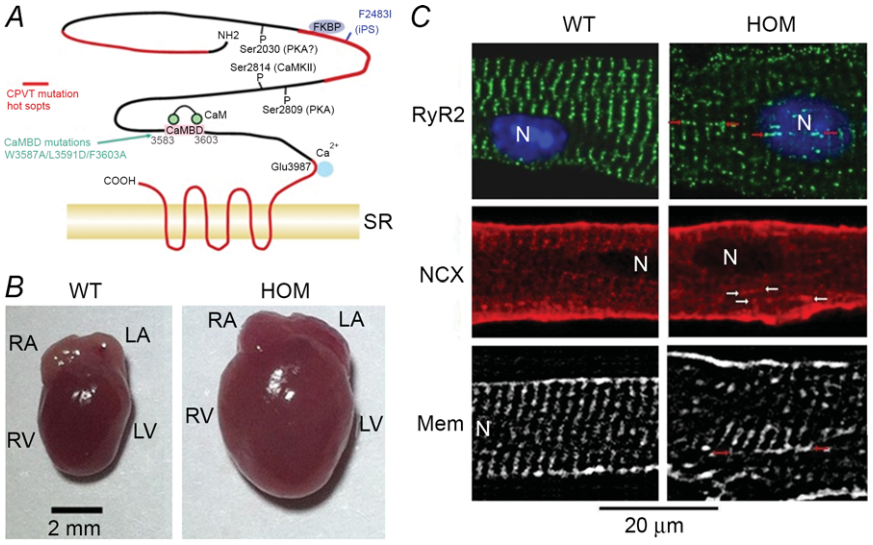

Figure 1. CaMBD of RyR2 (*A*) causes cardiac hypertrophy (*B*) and disorganized cellular structure (*C*)
A, location of the CaMBD in the context of binding domains for FKBP12.6 and Ca^{2+}, phosphorylation sites and hot spots for mutations causing catecholaminergic polymorphic ventricular tachycardia such as the F2431I mutation (Li & Chen, 2001; Lanner *et al.* 2010; Fatima *et al.* 2011). *B*, hypertrophy of hearts from HOM as seen at day 11 compared to WT. *C*, distributions of RyR2, NCX and Mem staining with voltage-sensitive dye (di-ANEPQ) in freshly isolated WT and HOM cardiomyocytes showing sarcomeric distributions with differing regularity and predominant localization of NCX at the surface membrane. It is noticeable that the ultrastructure of HOM cells is much less organized. Arrows in the right panel suggest that HOM cells have more prominent longitudinal tubules. Nuclei are marked with Ns and/or blue staining (top). CaMBD, calmodulin-binding domain; HOM, homozygous mutant mice; LA, left atria; LV, left ventricle; Mem, membrane; NCX, Na^{+}-Ca^{2+} exchanger; RA, right atria; RV, right ventricle; RyR2, type 2 ryanodine receptor; WT, wild-type.

I_{Ca}- and caffeine-induced Ca^{2+} release in mutant *vs.* wild-type mice

Cardiomyocytes from the WT and mutant mice were voltage clamped from holding potentials of −40 or −60 mV to avoid activation of residual I_{Na}, using step pulses to zero mV. Whole cell I_{Ca} and the accompanying Ca^{2+} transients activated by depolarizing pulses of 200–400 ms to 0 mV (Fig. 2*A* and *B*) were compared to those triggered by 2 s puffs of 5–10 mM of caffeine (Fig. 2*C* and *D*). Note that both the average rise in global cytosolic Ca^{2+} (Fig. 2*A* and *C*) and confocal images of Ca^{2+} distributions measured at 30 Hz (Fig. 2*B* and *D*) suggest a slower rise in cytosolic Ca^{2+} in mutant as compared to WT myocytes (Fig. 3). Interestingly, although the slower kinetics of Ca^{2+} release were also apparent in mutant myocytes in caffeine-triggered images of release of SR Ca^{2+} stores (compare confocal caffeine images, Fig. 2*D*), caffeine-triggered Ca^{2+} release was significantly larger and more sustained in mutant myocytes, and was accompanied by much larger I_{NCX} (Fig. 2*C*, see also Fig. 6*C* and *D*). Comparing the ratio of I_{Ca}-triggered Ca^{2+} release to the magnitude of caffeine-triggered Ca^{2+} release in mutant and WT myocytes (Fig. 2*E*) suggests that the efficiency of I_{Ca} to trigger Ca^{2+} release from the SR stores was significantly compromised in mutant myocyte, such that only about 30% of the stored Ca^{2+} is released in mutants compared to about 80% in WT myocytes.

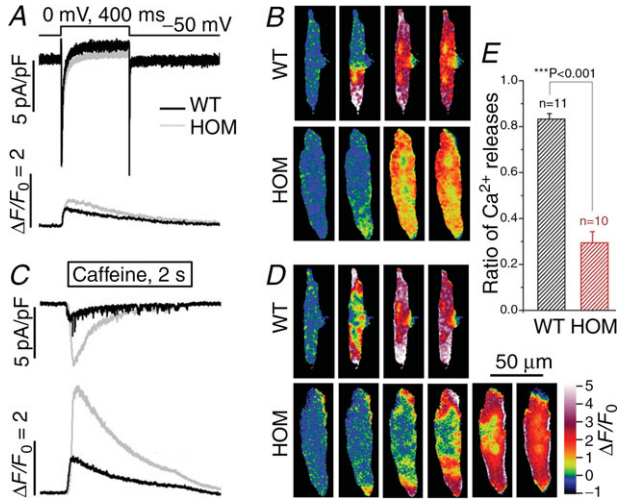

Figure 2. Ca^{2+} transients and membrane currents in single voltage-clamped cardiomyocytes from WT (black traces) and HOM (grey traces) mice
A, calcium transients (Fluo-4, $\Delta F/F_0$, bottom) evoked by activation of I_{Ca} (top) during 400 ms depolarizations to 0 mV. *B*, ratiometric confocal images ($\Delta F(x,y,t)/F_0(x,y)$) of Fluo-4 fluorescence measured at 30 Hz at the onset of the depolarization. The first frame in each sequence was recorded just before depolarization and shows a fairly uniform coloration over the entire cell with some blue/green mottle corresponding to the noise of the recordings. In the next frame, the WT cell shows an abrupt increase in fluorescence as a transition to warmer colours (See colour scale) yellow, half way through the 30 ms scan from top to bottom. In comparison, the second frame from the cardiomyocyte from the HOM mouse shows a delayed and gradual increase in fluorescence that starts at the edges, increases slowly towards the end of the scan and is still rising in the following two frames. *C*, I_{NCX} (top) and Ca^{2+} transients evoked by a 2 s application of 10 mM caffeine. *D*, ratiometric confocal fluorescence images indicate that Ca^{2+} signals evoked by caffeine start at the ends of the cells and rise more slowly than those triggered by I_{Ca}, especially in cells from the HOM mouse. *E*, ratio of the Ca^{2+} releases was calculated as the magnitude of depolarization-induced Ca^{2+} transients compared to those evoked by caffeine. This efficiency of I_{Ca}-gated Ca^{2+} release (fractional release) was significantly larger for WT (82%) than for HOM (30%) mice. The cells were dialysed with an internal solution containing 0.5 mM K_5Fluo-4 and 0.2 mM $CaCl_2$. HOM, homozygous mutant mice; WT, wild-type.

Voltage dependence of I_{Ca}-triggered Ca^{2+} release

Figure 3 compares sample records and the voltage dependencies of I_{Ca} and the I_{Ca}-triggered Ca^{2+} transients in control and mutant myocytes, showing similar bell-shaped voltage dependence for I_{Ca} and Ca^{2+} transients. There was, however, a clear difference in rate of activation of Ca^{2+} transients, such that they developed slower in mutant homozygote myocytes (Fig. 4). Although there was significant variability in the rate of relaxation of Ca^{2+} transients in mutant mice, there was a general tendency toward slower rates of relaxation in mutant myocytes, most likely related to the variability in the pathology of individual myocytes.

There was significant variability not only in Ca^{2+} transient kinetics between myocytes, but also in cell capacitance and I_{Ca} of both mutant and WT myocytes. Figure 5 compares the density of I_{Ca} in 37 WT and 52 mutant myocytes. I_{Ca} was significantly larger in WT (12–14-day-old mice) myocytes, about 12 pA/pF, compared to 6 pA/pF in mutant myocytes. Interestingly the smaller I_{Ca} (Fig. 6*C*) did not produce smaller I_{Ca}-triggered Ca^{2+} transients in mutant mice (Fig. 6*A*). This surprising finding may be, in part, related to the larger Ca^{2+} load of SR in mutant mice as indicated by three to four times larger caffeine-triggered Ca^{2+} transients, generating also the much larger I_{NCX} (Fig. 6*B* and *D*).

Figure 6*E* compares the gain of the I_{Ca}-triggered Ca^{2+} release (CICR) mechanism (i.e. the ability of I_{Ca} to release Ca^{2+} when corrected for the SR Ca^{2+} content) in the two sets of myocytes. We confirmed, as previously reported by a number of investigators, that the gain of CICR is significantly higher at −30 mV compared to 0 mV (Adachi-Akahane *et al.* 1996) in WT myocytes. In mutant myocytes, the gain was significantly smaller at both voltages, but the voltage dependence of gain of CICR was maintained.

Calcium sparks: kinetics, size and frequency

To gain more insight into the unitary activity of RyR2 in intact or patch-clamped myocytes from mutant mice, we compared the kinetics, frequency and the size of triggered or spontaneously occurring Ca^{2+} sparks with those of WT myocytes using a two-dimensional rapid confocal imaging system (Cleemann *et al.* 1998). Figure 7*A* and *B* shows that the frequency of spontaneously occurring sparks was significantly lower in mutant myocytes. This was especially unexpected as the Ca^{2+} load of SR was significantly larger in mutant myocytes (Fig. 6*B*). The number of sparks decreased from an average of 4 s^{-1} in control myocytes to 0.25 s^{-1} in mutant myocytes (Fig. 7*B*). Nevertheless, the rarely occurring spontaneous sparks in mutant mice were slow to develop and were of longer durations, lasting often for 250 ms (Fig. 7*E* and *F*). No significant difference was found in the amplitude of sparks in the two sets of myocytes (Fig. 7*D*).

Phosphorylation of Ca^{2+} signalling pathways

As a number of RyR2 mutations make this protein susceptible to irregular activity (George *et al.* 2007; Fig. 1), we tested whether $RyR2^{ADA}$ mutation altered the adrenergic regulation of I_{Ca} and I_{Ca}-triggered Ca^{2+} transients such as to increase the susceptibility of mutant mice to arrhythmogenesis and early death within 3 weeks of birth. We found that isoproterenol plus phosphodiesterase inhibitor IBMX significantly increased I_{Ca} and Ca^{2+} transients in a set of five mutant and control myocytes. There appeared to be no difference in qualitative or quantitative effects of isoproterenol between the two sets of myocytes (data not shown).

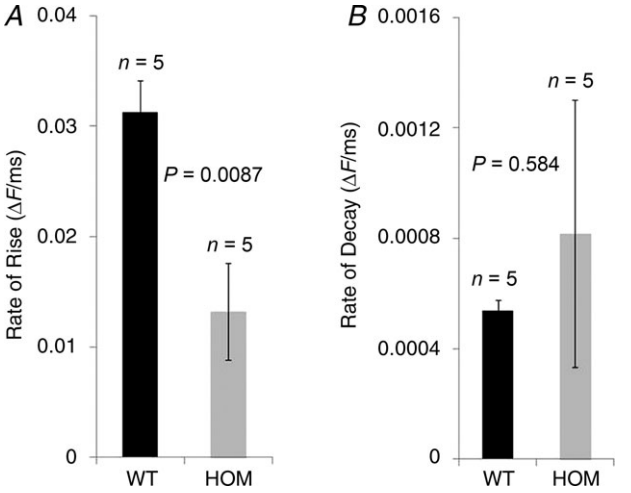

Figure 4. Average values of the rate of rise and decay of Fura-2-detected cytosolic Ca^{2+} transients measured during 400 ms depolarizations from −50 to 0 mV
A, rate of rise (ΔF/ms) was significantly slower in HOM than in the WT mice ($P < 0.01$). *B*, rate of decay showed considerable variation in the HOM mice, but on average was not significantly different from the WT. Ca^{2+}-sensitive fluorescence was measured using Fura2 dialysed cells (0.5 mM Fura2 and 0.5 mM Ca^{2+}. HOM, homozygous mutant mice; WT, wild-type.

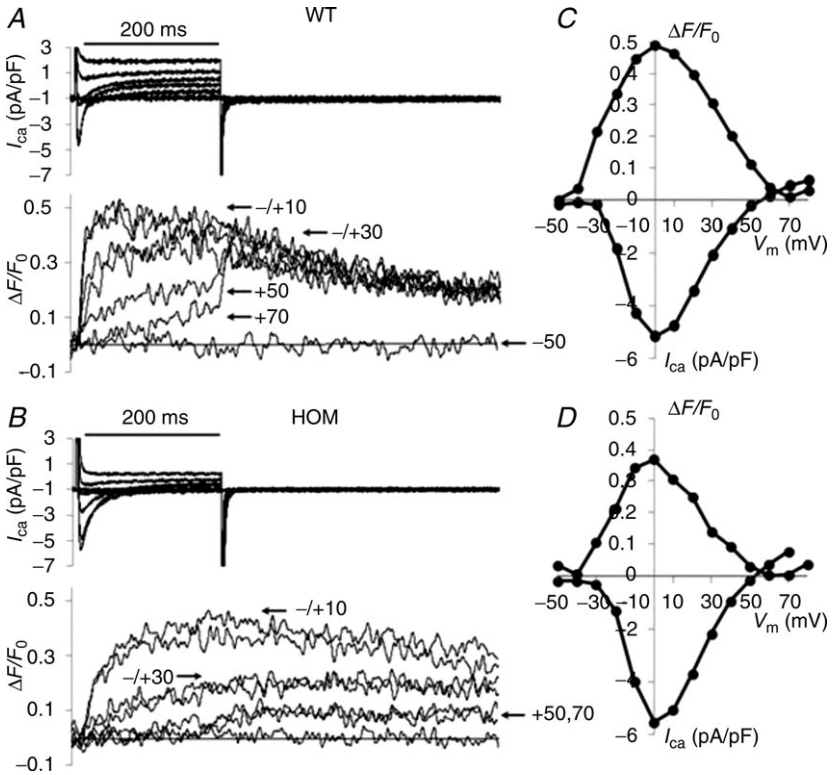

Figure 3. Voltage dependence of I_{Ca} and I_{Ca}-activated Ca^{2+} transients in cardiomyocytes from WT (*A* and *C*) and HOM (*B* and *D*)
A and *B*, representative traces where I_{Ca} was normalized relative to the membrane capacitance and changes in the Ca^{2+}-dependent fluorescence ($\Delta F/F_0$) was measured ratiometrically with Fura-2. The recordings were obtained with 200 ms depolarizing pulses from a holding potential of −50 mV in 10 mV steps to +70 mV. *C* and *D*, voltage dependencies of peak I_{Ca} and $\Delta F/F_0$. The internal solution contained 5 mM Na^+, and was Ca^{2+} buffered with 0.5 mM Fura-2, and 0.5 mM Ca^{2+}. HOM, homozygous mutant mice; WT, wild-type.

Alternans and activation of large Na^+-Ca^{2+} exchanger currents

It was a common finding that in a population of mutant, but never in WT myocytes, the Ca^{2+} release signal alternated between larger and smaller Ca^{2+} transients (Fig. 8*A*). The larger signal had two components, a rapid component triggered by I_{Ca} and a slower component that occurred spontaneously at variable times following the fast release of Ca^{2+} (Fig. 8*A*–*E*) and was always accompanied by large activation of I_{NCX}. Activation of the PKA–phosphorylation pathway often increased the proclivity for the occurrence of secondary Ca^{2+} releases and accompanying I_{NCX}, but there was significant inter-myocyte variability in occurrence of these large secondary Ca^{2+} release events to make the difference statistically insignificant (Fig. 8*F* and *G*).

Discussion

The major findings of this report are that genetically modified mice carrying $RyR2^{ADA}$ mutations express major Ca^{2+} signalling aberrancies in their freshly isolated hypertrophied ventricular cells that include: lower expression of I_{Ca} density and CICR gain; long-lasting but infrequent Ca^{2+} sparks; and slowly developing global Ca^{2+} transients despite the larger Ca^{2+} load of the SR.

Variability in myocyte size and Ca^{2+} signalling

There was significant variability in myocyte size and density of I_{Ca}, but on average the cell size (membrane capacitance) was larger and I_{Ca} smaller in the mutant than in control myocytes (Figs 1*C*, 2*B*, *D* and 5*D*). The myocytes' current and size variability, does not appear to reflect progression of cardiac pathology in the mutant mice as it was also present in the WT mice and may be, in part, related to the young age (10–15 days) of the mice, as previously reported in neonatal myocytes (Yan *et al.* 2011). Interestingly this variability did not extend to the size of caffeine-triggered Ca^{2+} stores. It was a hallmark of mutant myocytes that caffeine-triggered transients were consistently three to four times larger than the I_{Ca}-triggered Ca^{2+} transients producing markedly larger I_{NCX} of about 3–4 pA/pF compared to 0.8–1.0 pA/pF in WT myocytes (Fig. 6*B* and *D*). Although the presence of more disorganized structures and prominent longitudinal t-tubules in homozygous cardiomyocytes may reflect the greater fragility of mutant myocytes, it should be noted that these features were also observed not only in fixed and immunostained cells (Fig. 1*C*, RyR and NCX), but also in enzymatically dissociated live cells where membrane structures were visualized with di-2-ANEPEQ (Fig. 1*C*, Mem). To prevent experimental bias, most of Ca^{2+} signalling experiments were carried

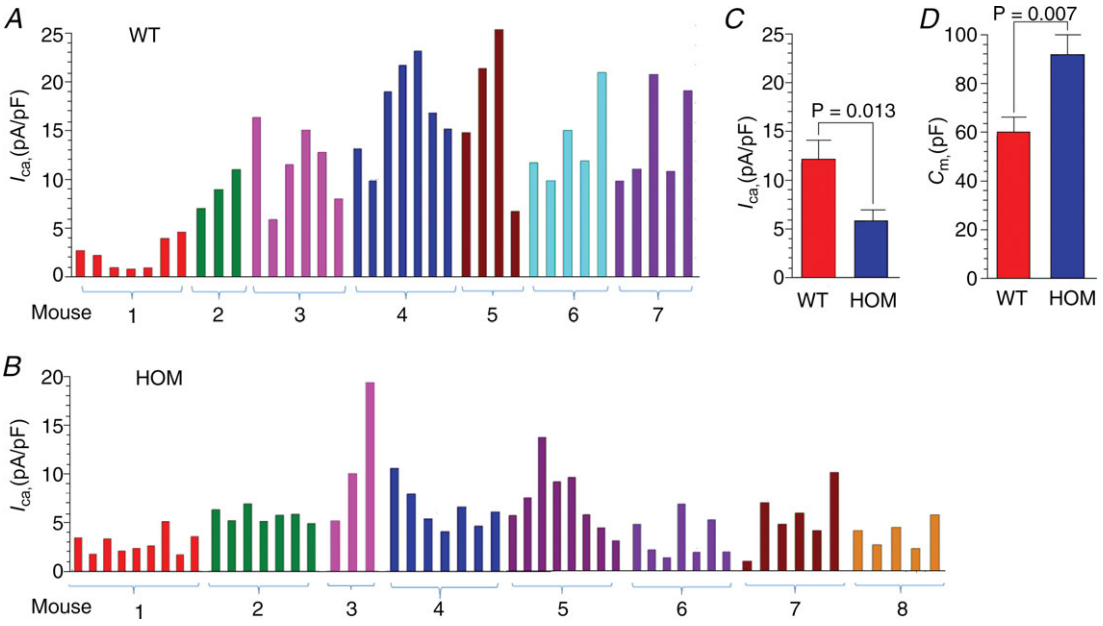

Figure 5. Distribution of calcium currents (I_{Ca}) density and average cell capacitance (C_m) in WT and HOM mice
I_{Ca} was recorded from a holding potential −50 mV with step depolarization to 0 mV. *A* and *B*, distribution of I_{Ca} densities in 37 cardiomyocytes from seven WT mice (*A*) compared to those in 52 cardiomyocytes from eight HOM mice (*B*). *C*, average I_{Ca} density was larger in WT than in HOM mice. *D*, average membrane capacitance of the cardiomyocytes was 60 ± 6 pF in WT myocytes compared to 92 ± 8 pF in the HOM myocytes. S.E.M. and thereby *P* values, in *C* and *D* are based conservatively on the numbers of experimental animals (seven and eight). HOM, homozygous mutant mice; WT, wild-type.

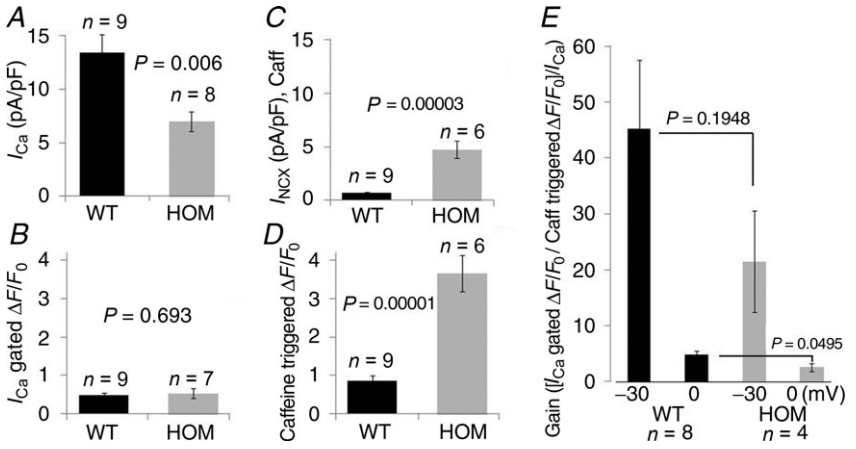

Figure 6. Average values of I_{Ca}, I_{NCX}, Ca_i transients (Fura-2 signals), and gain factor in WT and HOM mice myocytes
A and *C*, average Ca^{2+} signals (*A*) evoked I_{Ca} at 0 mV (*C*) in each group. *B* and *D*, average values of caffeine-activated Ca^{2+} signals (*B*) and the accompanying I_{NCX} (*D*) in each group. *E*, average valves of gain factor at −30 and 0 mV. The gain factor is plotted in units corresponding to the fraction (in %) of the caffeine-induced Ca^{2+} release, which is released by an I_{Ca} with a density of 1 pA/pF (WT black, HOM grey). Ca^{2+} transients were measured with Fura-2. HOM, homozygous mutant mice; WT, wild-type.

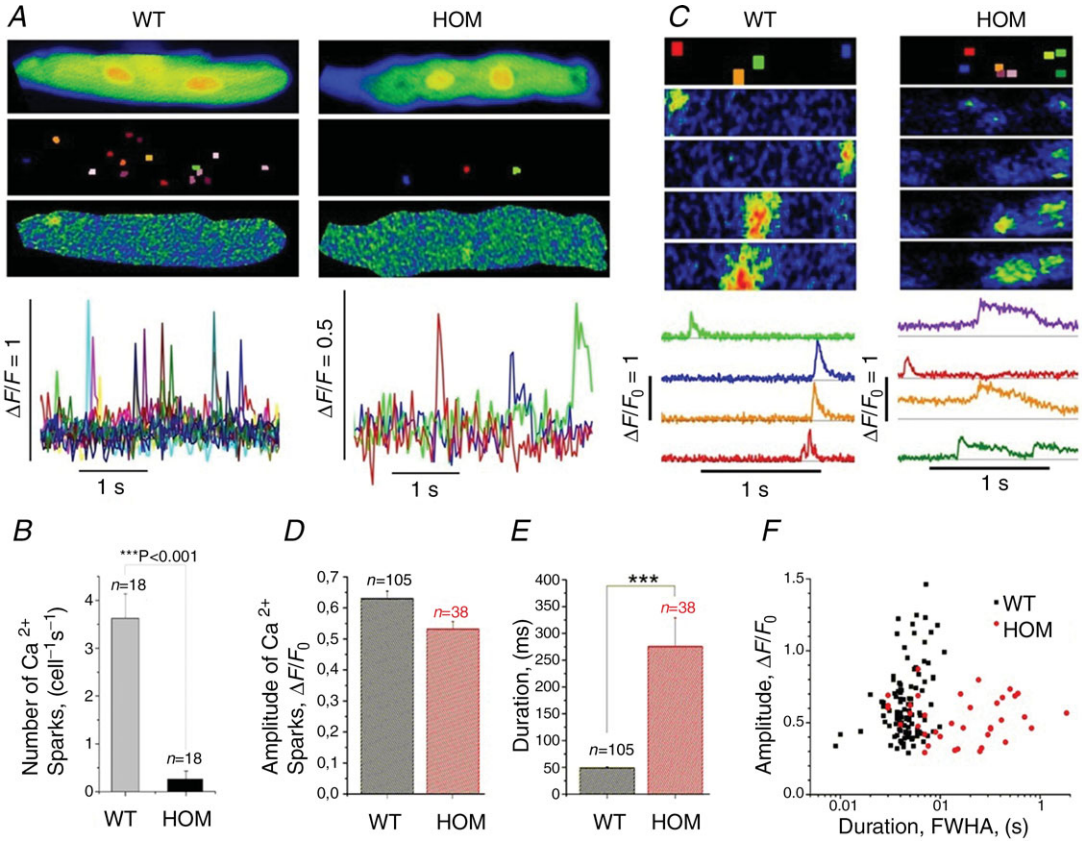

Figure 7. Calcium sparks in Fluo-4-dialysed voltage-clamped cardiomyocytes from WT and HOM mice
A, ratiometric recording of Ca^{2+} sparks in whole cells at 30 Hz. From top to bottom each panel shows: (1) images of the average fluorescence distributions in frames without Ca^{2+} sparks ($F_0(x,y)$); (2) colour-coded regions of interests corresponding to locations of Ca^{2+} sparks (middle panel); (3) examples of sparks as seen in single normalized frames ($\Delta F(x,y)/F_0(x,y)$), lower panel; and (4) the time course of the normalized fluorescence intensity at the chosen locations. *B*, number of sparks per cell per second was reduced from 3.62 ± 0.54per s in WT to 0.26 ± 0.17 per s in HOM cells. *C*, time course of Ca^{2+} sparks measured at 240 frames per s in portions of cells. At the top are shown colour-coded locations of Ca^{2+} sparks and sample frames with sparks at these locations. The traces below show the time course of $\Delta F/F_0$ in colour-coded traces corresponding to the chosen locations. For illustration purposes, we chose a rare mutant cell with several sparks that nevertheless was characteristic in having long durations. *D* and *E*, amplitude of the Ca^{2+} sparks are comparable in WT and HOM, but the duration is significantly longer in the HOM (FWHA). *F*, distribution of the sparks in the WT and the HOM according to $\Delta F/F_0$ and FWHA. FWHA, full width at half amplitude; HOM, homozygous mutant mice; WT, wild-type.

out blind, i.e. the mouse genotype was hidden from the experimenter.

Ca^{2+} signalling parameters: sparks, gain and store size

The most striking Ca^{2+} signalling phenotype of the freshly isolated mutant mice myocytes was that they had prolonged, but infrequent Ca^{2+} sparks, slowly developing and decaying Ca^{2+} transients and larger caffeine-triggered stores. The Ca^{2+} signalling profile of *Ryr2*^{ADA} mutant mouse heart has been summarized in Table 1. As previous measurements of [^{3}H]-ryanodine binding and single channel parameters showed significant differences between control and mutant RyR2 only in the presence of CaM (Yamaguchi *et al.* 2007), it is unlikely that other major 'unspecific' alterations in the channel conformation are induced by the mutation. This implies that the observed changes in Ca^{2+} signalling parameters are associated either directly with the loss of CaM-dependent inhibition of

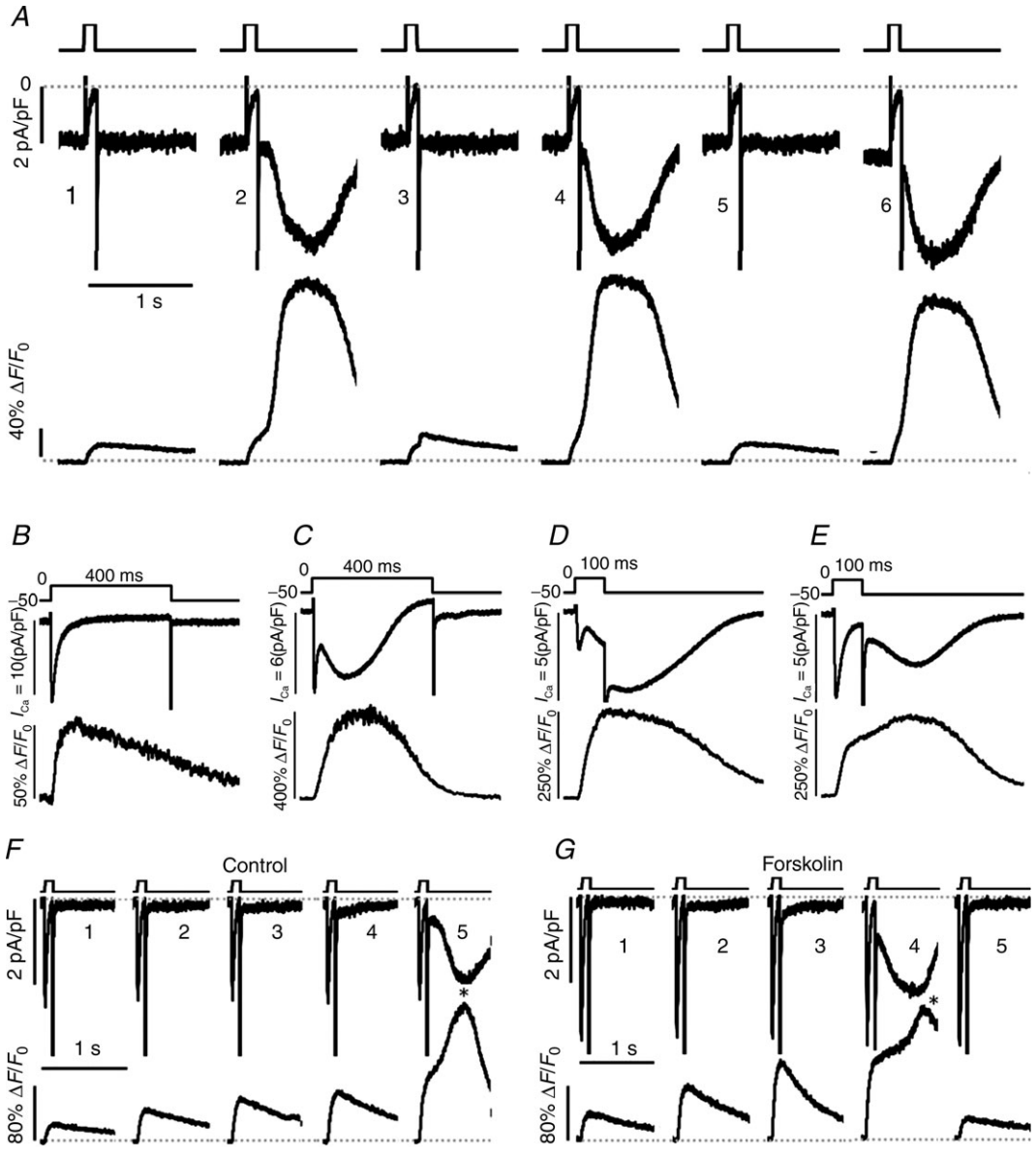

Figure 8. Spontaneous Ca^{2+} releases and associated I_{NCX} in cardiomyocytes from homozygous mutant mice
From top to bottom each panel shows voltage clamp depolarizations, membrane currents and cellular Ca^{2+} signals measured ratio metrically with Fura-2. *A*, six consecutive depolarizations at 0.2 Hz with alternating spontaneous large Ca^{2+} releases and I_{NCX}. *B–E*, cells with spontaneous Ca^{2+} releases and I_{NCX} with variable magnitudes and delays. *F* and *G*, cumulative effects of repeated depolarizations leading to large delayed Ca^{2+} releases before (*F*) and after (*G*) exposure to forskolin.

Table 1. Structural and functional changes in cardiomyocytes from homozygous mice expressing RyR2^{ADA}

		Wild-type → Mutant	Δ Change
Cell surface area, membrane capacitance		60 → 90 (pF)	↑
t-tubular structure		Disrupted	↓
I_{Ca} density		12 → 6 (pA/pF)	↓↓
I_{Ca}-triggered Ca^{2+} release gain	−30 mV		↓
	0 mV		↓↓
I_{Ca}-activated Ca_i transients	Amplitude		←→
	Kinetics		↓↓
Ca^{2+} load of sarcoplasmic reticulum			↑↑↑
SERCA 2A (uptake rate)		60% decrease	↓↓
Caffeine-triggered I_{NCX}		1 → 5 (pA/pF)	↑↑↑
Frequency of spontaneous Ca^{2+} releases			↑↑
Fractional Ca^{2+} release		80% → 30%	↓↓
RyR2 [^{3}H] ryanodine binding		70% decrease	↓↓↓
Ca^{2+} sparks	Frequency	3.5 s^{-1} → 0.3 s^{-1}	↓↓↓
	Duration	50 → 250 (ms)	↑↑
	Amplitude		←→

RyR2, type 2 ryanodine receptor.

RyR2 or with secondary compensatory changes in cellular structure and protein expression that in combination produce this lethal pathology.

The low frequency of Ca^{2+} sparks in cells with mutant RyR2s was surprising considering that the loss of CaM inhibition might be expected to increase the triggering of spontaneous Ca^{2+} releases. The lower spark frequency may result from a lower number of RyR2s, expressed in disorganized clusters (Yamaguchi *et al.* 2007) and by taking into account that CaM inhibition of channel activity is of little importance at the diastolic Ca^{2+} concentration that precede the formation of Ca^{2+} sparks. The long duration of the Ca^{2+} sparks in mutant cells (Fig. 7*E*), on the other hand, results most likely from the increased SR Ca^{2+} load and suppressed CaM-dependent inhibition (causing increased channel open probability; Yamaguchi *et al.* 2007), which comes into play only after a triggered Ca^{2+} spark causes an increase in the local Ca^{2+} concentration. The long duration of Ca^{2+} sparks is also consistent with the longer durations of Ca^{2+} transients reported in cultured homozygous neonatal cardiomyocytes (Yamaguchi *et al.* 2007) and with the idea that CaM binding to RyR2 regulates the termination of SR Ca^{2+} release (Xu & Meissner, 2004; Yamaguchi *et al.* 2007). The tendency for slower rates of decay of Ca^{2+} transients in mutant myocytes, but with larger S.E.M. (Fig. 4*B*), most likely arises from the possibility that the longer durations sparks may reactivate the couplons where dihydropyridine receptors and RyR2s are uncoupled because of cellular hypertrophy and t-tubular deformations. The degree to which such couplons are activated in time and space are likely to be responsible for slowly decaying Ca^{2+} transients (e.g. Fig. 8*B*), and possibly secondary releases of Ca^{2+} (Fig. 8*C–E*). It should be emphasized that the earlier reported measurements of Ca^{2+} signalling (Yamaguchi *et al.* 2007) were carried out on cultured myocytes where major changes in the t-tubular expression are known to occur that could have significant Ca^{2+} signalling consequences, especially when dealing with mutations causing myocyte hypertrophy. In summary, longer duration of Ca^{2+} sparks, one of the key findings in the present study using freshly isolated myocytes, is in good agreement with results from cultured myocytes (Yamaguchi *et al.* 2007) and the finding that spark frequency was significantly lower in mutant myocytes could be related to the lower expression of RyR2s, as indicated by ∼70% lower functional RyR2 proteins ([^{3}H]-ryanodine binding) and ∼30% decrease of mRNA in 10-day-old mice (Yamaguchi *et al.* 2007, see also Fig. 1*C*, RyR2 panels), or the deformities in t-tubules SR junctional membranes.

Although it is tempting to speculate that this lower spontaneous spark frequency was also responsible for the higher Ca^{2+} content of SR as suggested by the larger caffeine-triggered Ca^{2+} releases (Figs 2*C* and 6*B*), this possibility would be somewhat surprising considering the lower activity of Ca^{2+}-ATPase (SERCA2a/PLB) in the mutant mice (Yamaguchi *et al.* 2007). Closer examination of the Ca^{2+} release kinetics in mutant mice myocytes suggests often the presence of two components to Ca^{2+} release; the larger and slower of which follows the rapid and smaller I_{Ca}-triggered component of Ca^{2+} transients (Fig. 8*A*), suggesting possibly sites of release somewhat distal to the I_{Ca}-gated Ca^{2+} release. This finding could be related, in part, to uncoupled RyR2s that due to myocyte hypertrophy might have been dislocated from their t-tubular dyadic junctions and therefore from their direct gating by dihydropyridine receptors (Fig. 1*C*).

Pathophysiology of $RyR2^{ADA}$ mutation

Decreased CaM binding to RyR2 appears to be lethal to homozygote mice within the first 3 weeks of life. The impairment of cardiac function is already apparent in the first day of life where cardiac fractional shortening decreases from ∼50% in WT to ∼34% in homozygote mutant mice. Heterozygote mice survive into adulthood and appear to have little or no changes in fractional shortening, hypertrophy or Ca^{2+} signalling defects, as most of the tetrameric RyR2s carry at least one WT subunit, which is sufficient for CaM regulation (Yamaguchi *et al.* 2007). In considering the cause of early mortality in these mice, it has been proposed that massive hypertrophy and heart failure is the most likely cause of death. At day 1 of postnatal life, the left ventricular contractility is already reduced to ∼70% of WT and at day 10 it is down to ∼20% of WT hearts. Gene remodelling associated with cardiac hypertrophy was also detected in early embryonic day 16.5 hearts (Yamaguchi *et al.* 2007, 2011). In the present study, we suggest that, in addition to heart failure, arrhythmia may also contribute to the early death of the mutant mice. Considering the size of the mice and their hearts at this early stage of life, it was difficult to test directly their propensity for arrhythmia by telemetric ECG measurements. If indeed I_{Ca}-triggered release is followed by a secondary release of Ca^{2+}, as it is suggested by experiments in Fig 8, the large I_{NCX} generated by such releases would be highly arrhythmogenic in intact hearts *in vivo*, and could be responsible for the early death of the animal. Interestingly, we did not note an increase in proclivity to alternans or rhythm aberrancies when the mutant myocytes were subjected to β-adrenergic pathway agonists. Perhaps this is not surprising considering that the site of mutation was far removed from PKA-mediated phosphorylation sites.

The three- to four-fold increase in the caffeine-induced Ca^{2+} transients and I_{NCX}, reported here in freshly dissociated cardiomyocytes from homozygous mutant mice (Figs 2*B*, 6*C* and *D*), is somewhat at odds with the unchanged caffeine-induced Ca^{2+} transients previously reported in cultured neonatal homozygote cardiomyocytes (Yamaguchi *et al.* 2007). Perhaps this apparent discrepancy in the caffeine-induced Ca^{2+} transients is linked not only to differences in the experimental approach (cultured *vs.* freshly isolated cells), but also to dye saturation in the dye-incubated cells.

The larger Ca^{2+} load of the SR in mutant myocytes may also be responsible for the often-observed spontaneous releases of Ca^{2+} and its accompanying large I_{NCX} that followed I_{Ca}-triggered Ca^{2+} transients, which if occurring in intact hearts might activate early and delayed after depolarizations, leading possibly to lethal arrhythmia in the first 3 weeks of postnatal life. If indeed the pathology of $RyR2^{ADA}$ mice myocytes is linked to Ca^{2+} overload of the SR, but not necessarily to changes in 3-D ultrastructure, it is then possible that the cellular Ca^{2+} overload may also affect mitochondria rendering them incapable of buffering the large Ca^{2+} transients or contributing with a Ca^{2+} release of their own (Belmonte & Morad, 2008). Thus, the large caffeine-triggered rises in global Ca^{2+} may not be simply reflecting the true content of SR, but also that of Ca^{2+}-overloaded mitochondria. Such an idea is consistent with data of mutant hearts showing ∼60% decrease in SERCA2 Ca^{2+} uptake rates at day 10, more consistent with smaller rather than a larger SR Ca^{2+} content.

Somewhat similar hypertrophy was also reported in calsequestrin overexpressing mice (Jones *et al.* 1998; Knollmann *et al.* 2000) where the animals survived into adulthood. It should be noted, however, that calsequestrin overexpressing mice do not show heart failure in earlier (<2 months) stages of development, while in sharp contrast $RyR2^{ADA}$ hearts almost fail to have significant contractions at postnatal day 10, suggestive of different remodelling mechanisms. Indeed hypertrophy-induced gene expression and remodelling in $RyR2^{ADA}$ mice start in embryonic day 16.5, consistent with earlier cardiac remodelling and hypertrophy.

References

Adachi-Akahane S, Cleemann L & Morad M (1996). Cross-signalling between L-type Ca^{2+} channels and ryanodine receptors in rat ventricular myocytes. *J Gen Physiol* **108**, 435–454.

Anderson ME, Braun AP, Schulman H & Premack BA (1994). Multifunctional Ca^{2+}/calmodulin-dependent protein kinase mediates $Ca^{(2+)}$-induced enhancement of the L-type Ca^{2+} current in rabbit ventricular myocytes. *Circ Res* **75**, 854–861.

Balshaw DM, Yamaguchi N & Meissner G (2002). Modulation of intracellular calcium-release channels by calmodulin. *J Membr Biol* **185**, 1–8.

Belmonte S & Morad M (2008). 'Pressure-flow'-triggered intracellular Ca^{2+} transients in rat cardiac myocytes: possible mechanisms and role of mitochondria. *J Physiol* **586**, 1379–1397.

Cleemann L & Morad M (1991). Role of Ca^{2+} channel in cardiac excitation-contraction coupling in the rat: evidence from Ca^{2+} transients and contraction. *J Physiol* **432**, 283–312.

Cleemann L, Wang W & Morad M (1998). Two-dimensional confocal images of organization, density, and gating of focal Ca^{2+} release sites in rat cardiac myocytes. *Proc Natl Acad Sci U S A* **95**, 10984–10989.

Fatima A, Xu G, Shao K, Papadopoulos S, Lehmann M, Arnaiz-Cot JJ, Rosa AO, Nguemo F, Matzkies M, Dittmann S, Stone SL, Linke M, Zechner U, Beyer V, Hennies HC, Rosenkranz S, Klauke B, Parwani AS, Haverkamp W, Pfitzer G, Farr M, Cleemann L, Morad M, Milting H, Hescheler J & Saric T (2011). In vitro modelling of ryanodine receptor 2 dysfunction using human induced pluripotent stem cells. *Cell Physiol Biochem* **28**, 579–592.

Fill M & Copello JA (2002). Ryanodine receptor calcium release channels. *Physiol Rev* **82**, 893–922.

Franzini-Armstrong C & Protasi F (1997). Ryanodine receptors of striated muscles: a complex channel capable of multiple interactions. *Physiol Rev* **77**, 699–729.

George CH, Jundi H, Thomas NL, Fry DL & Lai FA (2007). Ryanodine receptors and ventricular arrhythmias: emerging trends in mutations, mechanisms and therapies. *J Mol Cell Cardiol* **42**, 34–50.

Hamill OP, Marty A, Neher E, Sakmann B & Sigworth FJ (1981). Improved patch-clamp techniques for high-resolution current recording from cells and cell-free membrane patches. *Pflugers Arch* **391**, 85–100.

Jones LR, Suzuki YJ, Wang W, Kobayashi YM, Ramesh V, Franzini-Armstrong C, Cleemann L & Morad M (1998). Regulation of Ca^{2+} signalling in transgenic mouse cardiac myocytes overexpressing calsequestrin. *J Clin Invest* **101**, 1385–1393.

Knollmann BC, Knollmann-Ritschel BE, Weissman NJ, Jones LR & Morad M (2000). Remodelling of ionic currents in hypertrophied and failing hearts of transgenic mice overexpressing calsequestrin. *J Physiol* **525** Pt 2, 483–498.

Lanner JT, Georgiou DK, Joshi AD & Hamilton SL (2010). Ryanodine receptors: structure, expression, molecular details, and function in calcium release. *Cold Spring Harb Perspect Biol* **2**, a003996.

Li P & Chen SR (2001). Molecular basis of Ca(2)+ activation of the mouse cardiac Ca(2)+ release channel (ryanodine receptor). *J Gen Physiol* **118**, 33–44.

Maier LS & Bers DM (2007). Role of Ca^{2+}/calmodulin-dependent protein kinase (CaMK) in excitation-contraction coupling in the heart. *Cardiovasc Res* **73**, 631–640.

Meissner G (1994). Ryanodine receptor/Ca^{2+} release channels and their regulation by endogenous effectors. *Annu Rev Physiol* **56**, 485–508.

Mitra R & Morad M (1985). A uniform enzymatic method for dissociation of myocytes from hearts and stomachs of vertebrates. *Am J Physiol Heart Circ Physiol* **249**, H1056–1060.

Saimi Y & Kung C (2002). Calmodulin as an ion channel subunit. *Annu Rev Physiol* **64**, 289–311.

Simmerman HK & Jones LR (1998). Phospholamban: protein structure, mechanism of action, and role in cardiac function. *Physiol Rev* **78**, 921–947.

Tang W, Sencer S & Hamilton SL (2002). Calmodulin modulation of proteins involved in excitation-contraction coupling. *Front Biosci* **7**, d1583–1589.

Xu L & Meissner G (2004). Mechanism of calmodulin inhibition of cardiac sarcoplasmic reticulum Ca^{2+} release channel (ryanodine receptor). *Biophys J* **86**, 797–804.

Yamaguchi N, Xu L, Pasek DA, Evans KE & Meissner G (2003). Molecular basis of calmodulin binding to cardiac muscle Ca(2+) release channel (ryanodine receptor). *J Biol Chem* **278**, 23480–23486.

Yamaguchi N, Takahashi N, Xu L, Smithies O & Meissner G (2007). Early cardiac hypertrophy in mice with impaired calmodulin regulation of cardiac muscle Ca release channel. *J Clin Invest* **117**, 1344–1353.

Yamaguchi N, Chakraborty A, Pasek DA, Molkentin JD & Meissner G (2011). Dysfunctional ryanodine receptor and cardiac hypertrophy: role of signalling molecules. *Am J Physiol Heart Circ Physiol* **300**, H2187–2195.

Yan X, Gao S, Tang M, Xi J, Gao L, Zhu M, Luo H, Hu X, Zheng Y, Hescheler J & Liang H (2011). Adenylyl cyclase/cAMP-PKA-mediated phosphorylation of basal L-type Ca(2+) channels in mouse embryonic ventricular myocytes. *Cell Calcium* **50**, 433–443.

Additional information

Competing interests

None.

Author contributions

J.J.A.-C. worked in the laboratories of the Cardiac Signaling Center in Charleston where he carried out voltage clamp and confocal Ca^{2+} and membrane imaging experiments and performed data analysis. B.D. worked in the laboratories of the Cardiac Signaling Center in Charleston where he carried out voltage clamp and whole cell Ca^{2+} measurements with Fura-2 and performed data analysis. X.-H.Z. worked in the laboratories of the Cardiac Signaling Center in Charleston where she carried out voltage clamp experiments, performed data analysis and contributed to the preparation of the final manuscript. L.C. worked in the laboratories of the Cardiac Signaling Center in Charleston where he took part in the design of experiments, confocal imaging studies and the drafting and revision of the manuscript. N.Y. worked first at the University of North Carolina, where he was instrumental in the creation and characterization of the mutant mice used in this study. More recently, he has worked in the laboratories of the Cardiac Signaling Center in Charleston where he has maintained a local colony of mutant and control mice, performed immunolabelling experiments and contributed to the drafting of the manuscript. G.M. works at the University of North Carolina, Chapel Hill, where he planned and supervised the creation and characterization of the RyR2 mutant mice used in this study. Lately he has contributed to the final revisions of the manuscript. M.M. works in the laboratories of the Cardiac Signaling Center in Charleston. He played a major role in the conception and design of the experiments and in the drafting of the manuscript. He has supervised the project and taken part in the analysis of and evaluation of data. All authors have approved the final version of the manuscript.

Funding

This study was supported by grants from the National Institutes of Health (R01 HL 15162 to MM, R03-AR061030 to NY, and R01 HL 073051 to GM), the American Heart Association (10SDG3500001 to NY) and the National Science Foundation (EPS-0903795 to NY).

Acknowledgements

The Π antibody to the Na^{+}-Ca^{2+} exchanger was generously provided by Dr Kenneth Philipson, UCLA. We thank Ms Susannah Stone for her unfailing help with isolation of mouse cardiomyocytes.